# An Experimental Investigation of the Stability of a Thin Liquid Layer Adjacent to a Supersonic Stream

WILLIAM S. SARIC* AND BILLY W. MARSHALL†
*Sandia Laboratories, Albuquerque, N. Mex.*

**The experiments to study the interface response of a liquid film with a concurrent supersonic airflow were conducted at freestream Mach numbers of 4.95 and 7.3 with stagnation pressures of 3.4, 6.8, and 17.0 atm. A sphere-cone and a blunt wedge were used as test configurations. The liquid layer Reynolds number $R$, based on interface velocity and liquid depth, ranged from approximately 0.3 to 300.0 as the thickness ranged independently from 0.01 to 0.05 cm. The nondimensional wave speed was found to decrease monotonically with increasing $R$ from a value greater than the interface velocity ("fast" waves) to a value lower than the interface velocity ("slow" waves). The transition from fast waves to slow waves appeared to occur at a Reynolds number near 100. The dependence of wavelength and wave speed on Reynolds number, shear stress, Mach number, and depth are given. In the small Reynolds number range, the results are compared with a long wave analysis to show the destabilizing effects of Reynolds number and shear stress. In the high Reynolds number range, the results are compared with an analysis based on a Tollmien-Schlichting instability mechanism.**

## Nomenclature

$c$ = dimensionless wave speed: $V/U$
$c_f$ = skin-friction coefficient: Eq. (6d)
$c_i$ = dimensionless amplification rate
$c_r$ = same as $c$
$F$ = Froude number: $U^2/gh$
$G$ = reciprocal Froude number: $1/F$
$g$ = body force per unit mass, cm/sec$^2$
$h$ = liquid layer depth, cm
$M$ = Mach number
$Q$ = volumetric flow rate, mliter/sec
$R$ = liquid Reynolds number: $Uh/\nu$
$T$ = reciprocal Weber number: $\alpha^2/W$
$U$ = interface velocity, cm/sec
$U_\infty$ = freestream velocity
$V$ = dimensional wave speed, cm/sec
$W$ = Weber number $\rho U^2 h/\sigma$
$\alpha$ = dimensionless wave number: $2\pi h/\lambda$
$\alpha_c$ = cutoff wave number: $c_i = 0$
$\Lambda$ = pressure perturbation: Eq. (6c)
$\lambda$ = wavelength, cm
$\nu$ = liquid kinematic viscosity, cm$^2$/sec
$\rho$ = liquid density, g/mliter
$\rho_\infty$ = freestream density, g/mliter
$\sigma$ = surface tension, dyne/cm
$\tau$ = interface shear stress, dyne/cm$^2$

## 1. Introduction

THE feasibility of using a transpiration cooling system to insure the maintenance of re-entry vehicle geometry and structural integrity from the effects of aerodynamic heating has received considerable interest recently. Essentially, the technique consists of injecting a liquid coolant in the stagnation region of a body and allowing the liquid to be swept back over the body, providing a protective liquid layer. Because of the consequences of losing this protection, the hydrodynamic stability of such a layer is of particular interest.

The character of the re-entry environment is such that the injected liquid is driven back by the shear forces exerted by the gas at the liquid-gas interface in the presence of heat and mass transfer at this interface. For certain parameters characterizing the liquid-gas flow, a wave motion will be initiated and subsequent liquid drop removal can occur. Gater and L'Ecuyer[1] have shown with a nearly incompressible gas flow that when this wave motion has occurred, the dominant liquid layer mass loss mechanism is the entrainment of liquid droplets into the airstream. Gold and his co-workers[2,3] have made calculations for the length of liquid layers on flat plates and sphere-cones at angle of attack using the subsonic results in the supersonic case.

The experiments reported on here were initiated in order to characterize in a fundamental way the response of a liquid layer interacting with a supersonic gas stream. This response is observed through the absence or presence of waves along with their shapes (two- or three-dimensional) and speeds (slower or faster than the interface velocity), thereby providing data on the nature of the interface as a function of liquid layer thickness, Reynolds number, Mach number and gas shear stress.

The interaction of an external gas with a liquid interface produces two important effects. The first is the establishment of a velocity profile in the liquid via an equilibrium force balance of the shear stress at the liquid-gas interface. The second effect is the initiation of perturbations in the normal and tangential stresses exerted by the gas on the interface due to the appearance of waves. Whereas the former effect can be stabilizing or destabilizing depending on a number of conditions, the latter effect leads to pressure perturbation (Kelvin-Helmholtz[4,5]) and shear perturbation[6-8] instability mechanisms.

If the external gas is inviscid and subsonic, flowing parallel to the undisturbed surface with a uniform mean velocity, the pressure perturbation is 180° out of phase with the surface wave. In this case, the gas pushes down at the troughs and sucks at the crests of the wave, thereby feeding energy to the disturbance in the liquid layer. In this model the effect of the axial component of the pressure perturbation is canceled. On the other hand, Miles[9] showed that if the external gas flow is

Presented as Paper 70-801 at the AIAA 3rd Fluid and Plasma Dynamics Conference, Los Angeles, Calif., June 29–July 1, 1970; submitted August 12, 1970; revision received April 21, 1971. This work was supported by the U.S. Atomic Energy Commission. The support and interest of C. C. Tolbert and A. A. Trujillo during the experiments is gratefully acknowledged. The authors also acknowledge their valuable discussions with A. H. Nayfeh on this paper.

Index Categories: Wave Motion and Sloshing, Multiphase Flows.

* Staff Member. Associate Member AIAA.
† Staff Member.

nonuniform, the pressure disturbance lags the wave by less than 180°. The axial component of the pressure perturbation can then do work on the wave. A different situation arises if the external flow is supersonic. Chang and Russell[5] showed that in this case, the pressure perturbation is in phase with the wave slope, giving rise to maximum energy transfer from the gas to the liquid through supersonic wave drag.

Nayfeh and Saric[10] showed that the cutoff wave numbers calculated by Chang and Russell for a subsonic flow were amplitude-dependent in the inviscid case, whereas they are amplitude-independent in the viscous case. For a supersonic flow and a viscous liquid, the cutoff wave number is amplitude-dependent. Moreover, their nonlinear analysis shows that stable linear disturbances die faster, whereas unstable linear disturbances achieve steady-state amplitude. Nachtsheim[11,12] extended the results of Chang and Russell by showing the importance of the liquid motion and the finite thickness liquid layer. Nayfeh and Saric[13] did a nonlinear analysis of Nachtsheim's model within the long wave approximation and found the cutoff wave number to be amplitude-dependent. Moreover, at small liquid layer Reynolds numbers, unstable disturbances do not grow indefinitely with time, but achieve steady-state amplitudes.

The analysis and experiments of Craik[6] with an incompressible air flow showed that thinner films may be more unstable than thicker films. This is so when the shear perturbation has a component in phase with wave slope. In effect, this shear component tends to pile up the liquid at the wave crests, a mechanism which becomes most effective when the liquid layer is very thin. The analysis of Nayfeh and Saric[14] extended the work of Nachtsheim and Craik by including an arbitrary body force and subsonic external flow using the long wave approximation. A simple relation between the wave speed and growth rate was also derived, which was useful in interpreting the experimental results presented below.

Miles[15] examined the possibility of instabilities arising from the disturbance Reynolds stress in the liquid near the wall. This is the so-called Tollmien-Schlichting instability mechanism. He found that at sufficiently large liquid Reynolds numbers, unstable disturbances could exist with propagation velocities less than the interface velocity. Heretofore, waves of this type have not been observed at high Reynolds numbers. The possibility of the existence of the Tollmien-Schlichting instability in the liquid layer is discussed in Sec. 3.1.

Experimental investigations of the stability of liquid films adjacent to concurrent subsonic airstreams have been conducted by Hanratty and Engen,[16] van Rossum,[17] Cohen and Hanratty,[18,19] Craik,[6] and Plate, Chang, and Hidy.[20] Except for Craik,[6] all of the experiments were conducted with relatively thick films (greater than 0.05 cm), unlike those that would be encountered under re-entry conditions. These thick film experiments show, like Craik's experiments, that increasing the liquid Reynolds number produces a transition from two-dimensional to three-dimensional waves; however, they do not show the three-dimensional waves at very low Reynolds number and very thin films. Little correlation is expected with their results, since in the present investigation, the shear levels are an order of magnitude higher and the external flow is supersonic. Since the experiments reported here have film thicknesses of the same order as Craik, most of the discussion will be centered around comparisons with his work.

**Table 1 Tunnel test conditions**

| Tunnel designation | I | II | III |
|---|---|---|---|
| Mach number | 4.95 | 4.95 | 7.3 |
| Total pressure, atm | 3.4 | 6.8 | 17.0 |
| Total temperature, °K | 800. | 800. | 800. |
| Reynolds number, $m^{-1} \times 10^{-6}$ | 1.56 | 3.12 | 2.87 |
| Freestream velocity, km/sec | 1.12 | 1.12 | 1.18 |
| Freestream density, g/mliter $\times 10^5$ | 13.8 | 6.9 | 6.2 |

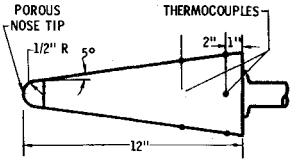


**Fig. 1 Sphere-cone model.**

## 2. Description of Experiments

The experiments were conducted in a hypersonic wind tunnel at Mach numbers of 4.95 and 7.3. The tunnel is a pebble-bed-heated, intermittent, blowdown-to-vacuum type with an 18-in.-diam, 48-in.-long test section. Test times were limited to 45 sec with a frequency of one per hour.

### 2.1 Models and Instrumentation

Two model configurations were used for the experiments. Figure 1 is a sketch of the sphere-cone model. The 1-in.-diam, hemispherical nose tips, manufactured with a special process by McDonnell Douglas, were made of porous stainless steel with permeability coefficients of $5 \times 10^{-10}$ and $1 \times 10^{-10}$ in.$^2$ Uniformity of the tips was assured since the variation in permeability was measured to be less than 7%. Six thermocouples were located as shown in Fig. 1 for measuring liquid temperature.

The second model configuration is shown in Fig. 2. A 1-in.-diam cylindrical nose tip is attached to the front of the plate. In order to insure that all of the liquid expelled through the nose tip is confined to the upper surface of the model, only the upper portion of the cylinder is made of porous material. The shaded region shown in Fig. 2 has an included angle of 75°. The porosity of this tip was $2.5 \times 10^{-10}$ in.$^2$ with the same tolerance on porosity as the hemispherical tips. Three thermocouples were mounted on the upper surface of the plate as shown in Fig. 2 for measurement of the liquid and plate temperatures. Approximately two-dimensional flow in the liquid was maintained by mounting side plates on the wedge. The sharp leading edges of the sides were located 0.5 in. in front of the nose tip and the sides extended 1.0 in. above the upper surface of the model. Based on a study of the photographic data, the thickness of the liquid was estimated to be uniform over the model except for a region very close to the sides where a thickness increase was noted. In addition, the motion of the waves was in the same direction as the gas motion and no lateral wave motion was observed. Based on these observations, it was concluded that if shock waves were present on the model as a result of the side walls, they did not create sufficiently strong adverse pressure gradients to cause any significant effect on the wave or liquid motion.

For both model configurations, the liquid was expelled through the tips by means of a high-pressure expulsion system. It consisted of a reservoir, filters, pressure monitoring

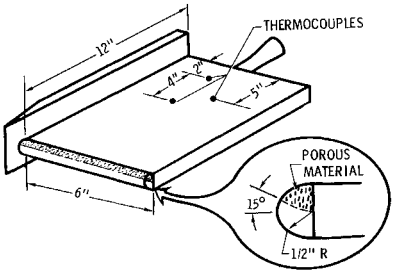


**Fig. 2 Wedge model.**

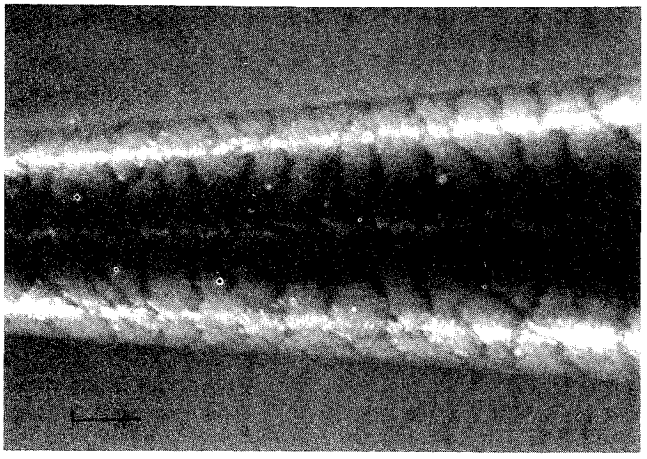

**Fig. 3 Water layer on sphere-cone model; $\tau$ = 190 dynes/cm² and $R$ = 100. Scale on figure is 1 cm.**

equipment and flow rate metering equipment. Pressure drops across the tips were held between 35 and 140 atm to prevent tunnel fluctuations and the spherical pressure distribution from affecting the flow rates. The flow rates were measured by recording the pressure drops across orifices that were calibrated for fluids of different viscosities.

During each run, the tunnel test conditions, the temperatures of the liquid and model, and the liquid flow rate were recorded on the tunnel computer data system. The interface response was photographed with high-speed 16 mm and 35 mm cameras. The 16 mm camera was a 400-frame/sec Millican, which uses color film, whereas the 35 mm camera was operated at 100 or 300 frame/sec using a fine grain black and white film. Timing marks were placed on the film to provide an accurate means of time resolution. The cameras observed the cone model through a side window in the tunnel in the presence of top, bottom, and front lighting provided by high-intensity tungsten lamps. The wedge, however, was observed from above with side and top lighting. The side plates on the wedge were made transparent in order to allow as much light as possible on the liquid surface.

The primary source of the data presented in this paper was the 35 mm motion pictures. By employing the timing marks on the film as reference times and the nose tip as a reference length, we used a Boscar film reader to measure the wave velocities and wave lengths from the film. After the image was projected on the screen of the reader, the continuously

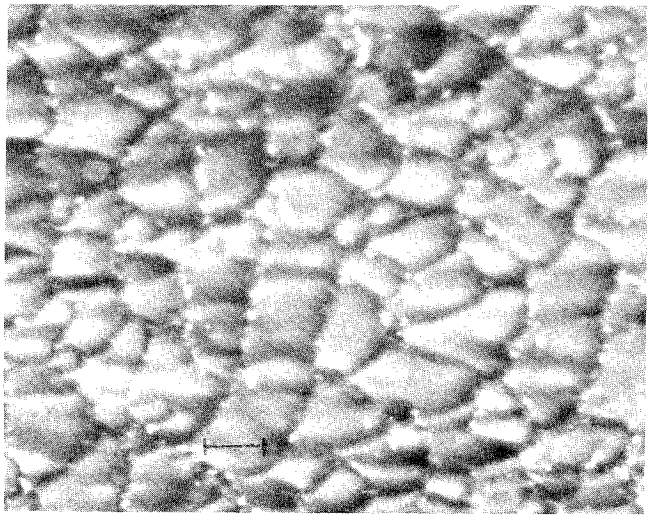

**Fig. 4 Water-glycerin layer on wedge; $\tau$ = 190 dynes/cm², $R$ = 40, $M$ = 5, and $\nu$ = 7 cp; flow from left to right. Scale on figure is 1 cm.**

adjustable cross hairs were used to locate a wave (chosen at random) and its position was traced from frame to frame. The reader keypunched the pertinent data on computer cards, which in turn were used in a desk computer to calculate the velocity and length of the wave. With this process, anywhere from 35 to 50 wave speeds were measured and averaged to obtain one datum point.

### 2.2 Test Conditions

The three tunnel conditions used to obtain the data reported on here are shown in Table 1. The external gas was air.

The Reynolds number of the liquid, based on interface velocity and liquid depth, was varied by changing the flow rate for any particular fluid. For a linear velocity profile in the liquid, the Reynolds number is given by

$$R = Uh/\nu = Q/k\nu \tag{1}$$

where $Q$ is the volumetric flow rate of the liquid; $\nu$ the kinematic viscosity, and $k$ a constant given by

$$k = \pi \cdot (\text{local cone radius}) \tag{2a}$$

or

$$k = \tfrac{1}{2} \cdot (\text{width of the flat plate}) \tag{2b}$$

The viscosity of the liquid was also varied in order to achieve an even wider range of depths and Reynolds numbers. Water and four different water-glycerin mixtures were used. They are listed in Table 2. The water-glycerin percentages are approximate and the viscosities were determined by a viscometer with the mixture at the test temperature. In all cases, blue, green, or black dye was added to the mixture to provide a better contrast for the photographic film. The variation in the surface tension caused by the addition of the dye was not measured, and nominal values for the appropriate glycerin-water mixtures were utilized in the analyses and data interpretation. It is well known that in the case of long waves such as those existing in these experiments, the stability criteria are relatively insensitive to the variation of the liquid surface tension. Therefore, the use of nominal surface tension values was considered acceptable.

The test matrix, shown in Table 3, was chosen to cover a wide range of Reynolds numbers while staying within the bounds of liquid thicknesses of 0.01–0.05 cm. In addition, the tunnel conditions permitted tests at different shear stress at the same freestream Mach number and tests at different freestream Mach number with the same shear stress. In Table 3, the lowest flow rate are lower limits for good model coverage during the test.

The gas boundary-layer conditions, such as shear at the interface and boundary-layer thickness, were calculated using the BLIMP computer program developed by Kendall and Bartlett.[21] The liquid conditions, such as depth and interface velocity, were calculated using the BLIMPL program developed recently by Grose and Kendall.[22] BLIMPL is a nonsimilar, variable property, boundary-layer solution based on BLIMP except that it is modified for liquid layers such as found in transpiration cooling systems. The water calculations are made by first running BLIMP under conditions of a gas over water where quasi-steady equilibrium is assumed between the liquid and the gas at the interface. Interfacial

**Table 2 Test liquids**

| Fluid designation | % water/ glycerin | Density, g/mliter | Viscosity, centipoise |
|---|---|---|---|
| A | 100/0 | 1.0 | 1.3 |
| B | 40/60 | 1.15 | 7.0 |
| C | 25/75 | 1.18 | 15.0 |
| D | 15/85 | 1.21 | 35.0 |
| E | 0/100 | 1.26 | 70.0 |

shear and mass transfer along with equilibrium temperature are calculated. These results are then used as input to BLIMPL, which in turn calculates the velocity and temperature distributions in the liquid. Depending on the wall conditions of the liquid and the amount of blowing, an iterative procedure can be carried out between the two programs to get the correct results. In the results that follow, only nominal values of the shear stress are quoted.

The boundary layer was assumed to be laminar for the test conditions of Table 1 since estimates for the gas transition Reynolds number were always an order of magnitude greater than the boundary-layer edge Reynolds number. For the cone, the transition Reynolds number ranged from $6 \times 10^6$ to $8 \times 10^6$ and the edge Reynolds number calculated at the base ranged from $0.2 \times 10^6$ to $0.4 \times 10^6$. For the wedge, the transition Reynolds number was about one-half of the cone values, whereas the edge Reynolds number was approximately 20% lower than the cone values. The effects of free-stream Mach number,[23] tunnel size,[23] wall to recovery temperature ratio,[24] and nose bluntness[25-27] were taken into consideration in making these estimates. The effect of the liquid layer and the surface waves on transition are still matters of conjecture.

Mass entrainment was not included in any of the calculations because of the very low dynamic pressures of the gas stream. Had we applied the correlation of Gater and L'Ecuyer following Gold, we predict entrainment on the order of 2% for the extreme tunnel condition which is well within the experimental error. In fact, the mass transfer due to the low tunnel pressure was far more significant.

## 3. Discussion of Results

### 3.1 Comparison of Wave Characteristics

Figure 3 is a print from the 35mm film of the cone at test number 26 (see Table 3). The liquid is water at a Reynolds number of 100. The waves are clearly axisymmetric and they move at a velocity of 106 cm/sec, which is slower than the interface velocity, calculated to be 125 cm/sec. The slight asymmetries in the wave patterns are due to the presence of gravity directed transverse to the axis of the cone. The liquid is slightly thicker on the bottom, which gives rise to a higher wave speed. The edge of the photo represents an axial location of 9.0 nose radii from the tip. Figures 4 and 5 are prints from tests 4 and 13, respectively. They illustrate the effects of the external gas conditions on the interface wave structure. The waves in Fig. 4 possess longer lateral

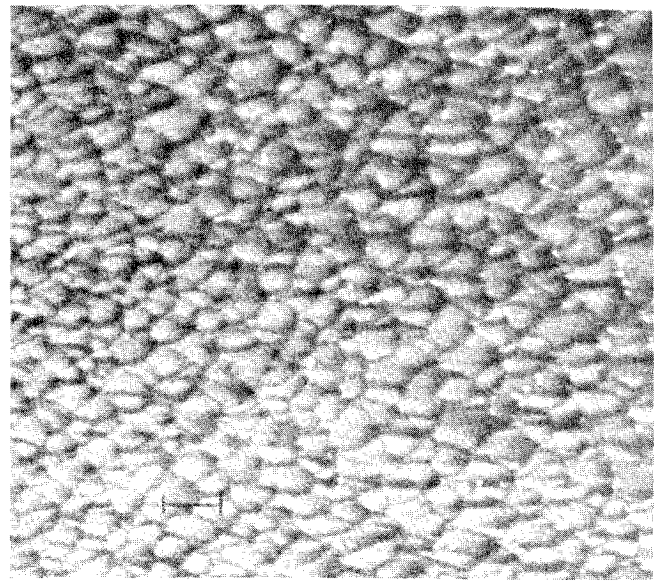

**Fig. 5 Water-glycerin layer on wedge; $\tau = 240$ dynes/cm², $R = 40$, $M = 5$, and $\nu = 7$ cp; flow from left to right. Scale on figure is 1 cm.**

**Table 3 Calculated test conditions**

| Model | Test number | Tunnel designation (Table 1) | Liquid designation (Table 2) | Flow rate, mliter/sec | Film thickness, cm | Interface velocity, cm/sec | Shear stress, dyne/cm² | Reynolds number $Uh/\nu$ | Weber number $\rho U^2 h/\sigma$ | Froude number $U^2/gh$ |
|---|---|---|---|---|---|---|---|---|---|---|
| | | Test conditions | | | | Calculated conditions | | | | |
| | 1 | I | E | 2.42 | 0.031 | 9.8 | 200 | 0.5 | 0.052 | 3.16 |
| | 2 | · | B | 4.22 | 0.015 | 39.6 | 200 | 9.0 | 0.41 | 102.0 |
| | 3 | · | B | 10.5 | 0.024 | 67.0 | 200 | 22.5 | 1.796 | 191.0 |
| | 4 | · | B | 19.0 | 0.031 | 82.2 | 170 | 40.0 | 2.91 | 222.0 |
| | 5 | · | A | 10.1 | 0.010 | 155.0 | 190 | 120.0 | 3.34 | 2452.0 |
| | 6 | · | A | 12.2 | 0.013 | 164.0 | 185 | 140.0 | 4.86 | 2111.0 |
| | 7 | · | A | 15.8 | 0.014 | 189.0 | 170 | 195.0 | 6.95 | 2604.0 |
| | 8 | II | E | 1.58 | 0.024 | 9.1 | 260 | 0.33 | 0.035 | 3.52 |
| | 9 | · | E | 2.42 | 0.025 | 12.2 | 290 | 0.5 | 0.065 | 6.08 |
| Wedge | 10 | · | B | 4.22 | 0.013 | 45.7 | 260 | 9.0 | 0.453 | 164.0 |
| | 11 | · | B | 7.88 | 0.018 | 61.0 | 260 | 17.0 | 1.12 | 211.0 |
| | 12 | · | B | 10.5 | 0.020 | 76.0 | 250 | 22.5 | 1.93 | 295.0 |
| | 13 | · | B | 19.0 | 0.027 | 96.3 | 260 | 40.0 | 4.0 | 351.0 |
| | 14 | III | E | 1.58 | 0.028 | 8.5 | 190 | 0.33 | 0.035 | 2.63 |
| | 15 | · | E | 2.42 | 0.033 | 9.1 | 180 | 0.5 | 0.048 | 2.56 |
| | 16 | · | B | 10.45 | 0.023 | 64.0 | 180 | 22.5 | 1.57 | 182.0 |
| | 17 | · | A | 10.5 | 0.010 | 149.0 | 180 | 120.0 | 3.1 | 2265.0 |
| | 18 | · | A | 11.9 | 0.011 | 161.0 | 190 | 136.0 | 4.0 | 2404.0 |
| | 19 | · | A | 15.6 | 0.013 | 184.0 | 180 | 179.0 | 6.11 | 2657.0 |
| | 20 | · | A | 22.6 | 0.015 | 216.0 | 160 | 260.0 | 9.85 | 3132.0 |
| | 21 | I | D | 1.2 | 0.021 | 19.0 | 150 | 0.55 | 0.133 | 17.5 |
| | 22 | · | A | 15.8 | 0.015 | 218.0 | 135 | 225.0 | 9.9 | 3233.0 |
| Sphere-cone | 23 | II | D | 1.33 | 0.017 | 19.0 | 190 | 0.6 | 0.107 | 21.7 |
| | 24 | · | C | 2.25 | 0.016 | 20.0 | 190 | 3.0 | 0.102 | 25.5 |
| | 25 | · | B | 7.9 | 0.020 | 61.0 | 190 | 20.0 | 1.19 | 190.0 |
| | 26 | · | A | 7.9 | 0.015 | 125.0 | 190 | 100.0 | 3.26 | 1063.0 |
| | 27 | · | B | 7.9 | 0.023 | 70.0 | 260 | 24.0 | 1.8 | 217.0 |

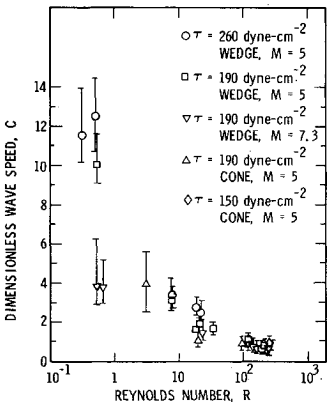


**Fig. 6 Dimensionless wave speed vs Reynolds number. Error bars indicate extremes of all data.**

spans and larger wavelengths than the waves shown in Fig. 5. This change was made to occur by increasing the interface shear and keeping all other parameters the same. Although the waves in Fig. 4 are interconnected and are also distorted and curved, they are not as irregular as the waves shown in Fig. 5. In Fig. 4, individual waves can be identified, whereas in Fig. 5 the dominant feature is one of a totally interconnected pattern of smaller waves. The irregular waves on the cone were identical in appearance to those shown in Fig. 5 except for a longer wavelength. As a rule, the wedge had a greater tendency to have irregular waves than the cone under identical test conditions. This is due in part to the different external flowfields, surface pressure, and the larger span of the wedge. All waves observed can be classified as long waves. That is, the dimensionless wavelength, given as the dimensional wavelength normalized by the liquid depth ($\lambda/h$), is a large number.

Figure 6 shows the dimensionless wave speed $c$ as a function of Reynolds number. The measured wave speeds $V$ were normalized with the interface velocity $U$ obtained from the calculations described in Sec. 2.2. Each datum point in Fig. 6 represents an arithmetic average of 35–50 film readings taken at various times during the run. The irregular fast waves resembled those of Fig. 5 and are discussed in Sec. 3.2. The slow waves appeared aperiodic, and it was very difficult to determine a characteristic wavelength beyond the Reynolds numbers shown. Since low Reynolds number data were obtained by using the larger viscosity mixtures, the thickness was substantially larger for low Reynolds number data than for the high Reynolds number data. This can be seen for a linear velocity profile where

$$\tau = \rho\nu\ U/h = \rho U^2/R = \rho(\nu/h)^2 R \qquad (3)$$

with $\tau$ the interface shear. Equation (3) shows that changes in viscosity with $R$ and $\tau$ fixed may also be interpreted as depth effects and vice versa.

The interesting result here is the presence of slow waves in a high Reynolds number, small thickness regime. Here, slow waves are defined as waves moving at a velocity which is less than the calculated interface velocity of the liquid, i.e., $c < 1$. All of the large Reynolds number data of Craik[6] and Cohen and Hanratty[18] showed fast waves ($c > 1$), although Craik's values of $R$ did not extend to the extreme values of Cohen and Hanratty or to those presented here where $c < 1$. Cohen and Hanratty[18] also did an analysis valid for large Reynolds numbers by using the method outlined by Miles[8] for calculating the stress perturbations on the interface. They only considered solutions where $c > 1$ and thus were able to correlate these results with the experimental observations. Since the observation of slow waves is a significant result, it appears that there are a number of important considerations which must be addressed in order to explain their appearance in our experiments.

First, it is appropriate to mention the reliance on the complicated boundary-layer calculations described in Sec. 2.2. A gross overestimation of the interface velocity could be giving misleading results. However, since the nominal values of the dimensionless wave speeds are in the neighborhood of 0.7, to place most of the wave speed data above $c = 1.0$, the calculated interface velocity must be 1.4 times the actual interface velocity. This means that the calculated shear stress must be twice the actual shear stress. This error could come from the inability to predict the shear for the undisturbed liquid flow or from a change in the shear stress field due to the appearance of waves, or both. Although an error of this magnitude seems unlikely for laminar boundary-layer calculations, it is probable that the calculations contain some inaccuracies. However, it is not thought that this alone constitutes the complete explanation of the data.

A plausible source of slow waves is the Tollmien-Schlichting instability mechanism proposed by Miles[15] for liquid layers that may be operative in this range of Reynolds numbers. That is, the unstable disturbances receive their energy from the mean flow of the liquid rather than from the gas. The disturbances receive their energy from the mean flow of the liquid or the gas depending on whether the wave speed is less than or greater than the interface velocity. Miles concluded that a necessary condition for instability, assuming a Tollmien-Schlichting mechanism, is

$$R > 203 \quad \text{and} \quad 1/W + 1/\alpha^2 F < \tfrac{1}{3} \qquad (4)$$

where $R$, $W$, and $F$ are the Reynolds, Weber, and Froude numbers defined in Table 3 and $\alpha = 2\pi h/\lambda$ is the dimensionless wave number. The condition on $W$ and $F$ is satisfied for over half of the slow wave cases, whereas the inception of slow waves occurred near $R = 100$. Therefore, Eq. (4) is in agreement at least within an order of magnitude with the experiments. Examination of the data of Fig. 6 reveals a subtle, monotonic change in dimensionless wave speed with changes in $R$. However, in examining Fig. 7, which shows the variation of the dimensional wave speed $V$ with $R$, it is apparent that in the region of $R = 100$, there is a definite "dog-leg" in the data, which further suggests a change in wave behavior. The $c > 1$ mechanism of Cohen and Hanratty[18] apparently becomes inoperative in these experiments at high Reynolds numbers. Both the higher shear stress and the thinner layer contribute to a greater viscous dissipation at the interface, which tends to reduce the destabilizing effects of the stress perturbations and allow disturbances to receive their energy from the average velocity profile in the liquid. In addition, the shear perturbations are being reduced as $1/R$, while compressibility effects may be modifying the velocity profiles and values of skin friction to the point where the models of Miles[9] or Craik-Benjamin[7,6] are no longer applicable.

Another explanation of the existence of slow waves is the nonlinear motion of the liquid layer. Craik[22] showed that this nonlinear motion reduces the wave speed to a value that

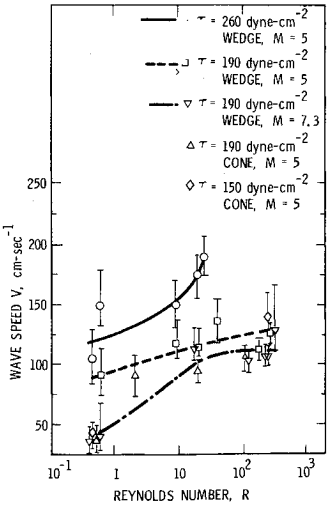


**Fig. 7 Dimensional wave speed vs Reynolds number. Solid, dashed, and dash-dot lines are trends of data.**

is smaller than the interface velocity and hence could be an operative mechanism in this range of Reynolds numbers. In fact, in the face of other experimental data, one would be more likely to assume that this is the case rather than the Tollmien-Schlichting instability. However, if the Reynolds number is increased beyond the largest values of Table 3, no discernible wave pattern is apparent. High-speed motion pictures show the motion of the liquid to be chaotic and random, suggesting a turbulent motion in the liquid layer. By analogy to boundary-layer stability, this apparent transition to turbulence makes the conjecture of a Tollmien-Schlichting mechanism more plausible.

Although the evidence is far from conclusive, the preceding observations suggest that the Tollmien-Schlichting mechanism may be the dominant mechanism. Further experimental work should be directed toward including detailed flowfield measurements which could answer some of the questions raised here.

### 3.2 Comparison of Fast Waves with Theory

It is generally recognized that the Kelvin-Helmholtz instability is likely to occur with an airflow over a very viscous liquid.[4] It is possible to examine the behavior of the fast waves observed here by using the physical model of Nachtsheim[11,12] described in Chap. 1. That is, the external gas is assumed inviscid and supersonic and its essential effects are to produce the mean shear flow in the liquid and to support pressure perturbations that are in phase with the wave slope. The shear perturbation model of Craik is probably not important here because of the relatively thick layers and the large values of the pressure perturbation in the gas.

The calculations of Nachtsheim required the numerical solution of the Orr-Sommerfeld equation, and his results were presented for conditions of fixed Weber and Froude numbers which are not met in the experiments reported on here. Therefore, a different solution technique is employed. As an extension of Nachtsheim's work, Nayfeh and Saric[13,14] developed approximate solutions for long wavelengths for the linear and nonlinear problems. The disturbance stream function was solved for by assuming a perturbation solution in powers of the dimensionless wave number $\alpha$.

The linear solutions for the dimensionless wave speed $c_r$ and the dimensionless amplification rate $c_i$ are[14]

$$c_r = 1 + \frac{1}{3}\Lambda - \frac{2}{15}\alpha R\Lambda c_i - \frac{3}{5}\alpha^2\Lambda - \frac{1}{30}\alpha^2R^2\left\{\frac{13}{12}(T-G) + \frac{823}{6048}\Lambda - \left[4(T-G) + \frac{205}{224}\Lambda\right]c_r + \frac{34}{21}(c_r^2 - c_i^2)\right\} + \frac{47}{90}\alpha^3R\Lambda c_i + \frac{1}{5040}\alpha^3R^3c_i\left\{\frac{1551}{10}(T-G) + \frac{1021}{36}\Lambda - \left[3808(T-G) + \frac{3439}{18}\Lambda\right]c_r + \frac{39923}{360}\Lambda(3c_r^2 - c_i^2)\right\} + 0(\alpha^4) \quad (5a)$$

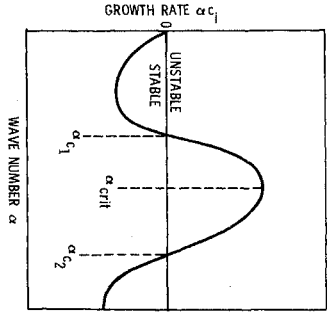


**Fig. 8 Behavior of growth rate as a function of wave number.**

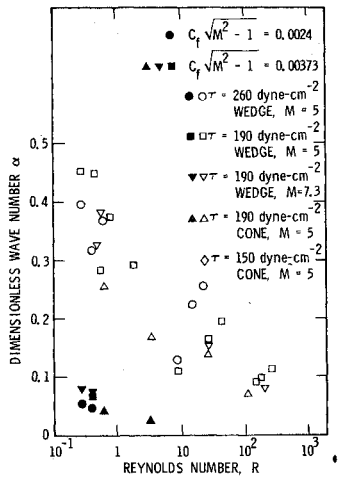


**Fig. 9 Comparison of measured wave numbers with theory at different Reynolds numbers. Solid symbols and lines are calculations with Eq. (5).**

$$c_i = -\frac{1}{3}\alpha R\left(T - G + \frac{13}{120}\Lambda - \frac{2}{5}\Lambda c_r\right) + \frac{2}{15}\alpha^2R^2c_i\left(T - G + \frac{205}{896}\Lambda - \frac{17}{21}\Lambda c_r\right) + \frac{1}{45}\alpha^3R\left[27(T-G) + \frac{101}{14}\Lambda - \frac{47}{2}\Lambda c_r\right] + \frac{1}{5040}\alpha^3R^3\left\{\frac{143}{6}(T-G) + \frac{6917}{2376}\Lambda - \left[\frac{1551}{10}(T-G) + \frac{1021}{36}\Lambda\right]c_r + \left[1904(T-G) + \frac{3439}{36}\Lambda\right](c_r^2 - c_i^2) - \frac{39923}{360}\Lambda(c_r^3 - 3c_rc_i^2)\right\} + 0(\alpha^4) \quad (5b)$$

where

$$T = \frac{\sigma}{\rho U^2 h}\alpha^2 = \frac{\sigma}{\nu}\left(\frac{1}{\tau R^3\rho}\right)^{1/2}\alpha^2\text{: reciprocal Weber number} \quad (6a)$$

$$G = \frac{gh}{U^2} = \nu g\left(\frac{\rho^3}{\tau^3 R}\right)^{1/2}\text{: reciprocal Froude number} \quad (6b)$$

$$\Lambda = \alpha^2/c_f(M^2-1)^{1/2}\text{: pressure perturbation} \quad (6c)$$

$$c_f = \tau/\rho_\infty U_\infty^2\text{: friction coefficient} \quad (6d)$$

The body force per unit mass is directed from the liquid to the gas and the rest of the notation is standard. The unusual forms of $T$ and $G$ are from Eq. (3) and reflect the experimental conditions. That is, $\tau$ is an external gas condition and $R$ is proportional to the flow rate; therefore, $T$ and $G$ are not independent parameters. Once the fluid properties are fixed, $R$ and $\tau$ are the remaining independent parameters. The behavior of the disturbance growth rate $\alpha c_i$, calculated from Eq. (5b) for this model, is illustrated in Fig. 8. This is essentially a frequency response curve for the case of infinitesimal initial conditions. The small wave number disturbances are stable due to the shear in the liquid and the body force directed from the gas to the liquid. The very large wave number disturbances are stable because of the stabilizing effects of surface tension. The intermediate region, bounded by the cutoff wave numbers $\alpha_{c_1}$ and $\alpha_{c_2}$, is the region of unstable modes where we expect our observed wave numbers to lie. The comparison of the solutions of Eq. (5) with a numerical solution of the complete problem shows

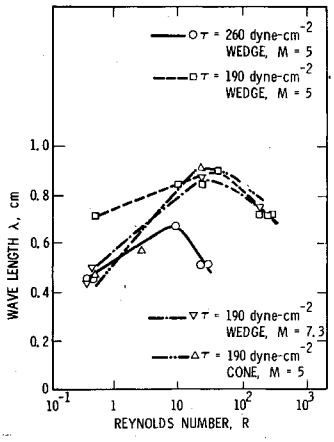


**Fig. 10 Wavelength vs Reynolds number. Solid, dashed, and dash-dot lines are trends of data.**

that Eq. (5) can correctly predict the first cutoff wave number. In addition, it can predict the amplification rate and wave speed for wave numbers slightly larger than this cutoff wave number.[14]

Figure 9 is a comparison of the experimentally observed wave numbers with the first cutoff wave number calculated from Eq. (5b). Two important features can be noted. First, all of the observed wave numbers are greater than the calculated cutoff values and hence are in the unstable range indicated in Fig. 8. For most of the cases, numerical solutions of the complete eigenvalue problem show that the maximum growth rate occurs at $\alpha_{crit} = O(3)$ and that the second cutoff wave number occurs at $\alpha_{c_2} = O(10)$ so that on a relative scale, the observed values are the same order of magnitude as the cutoff values. The nonlinear analysis of Nayfeh and Saric[13] indicates that a finite amplitude has a stabilizing effect and that unstable disturbances do not grow indefinitely with time but achieve steady-state amplitudes.

The second observation is the ability of the linear theory to correctly predict the destabilizing trends of the shear and Reynolds number. As the cutoff wave number is decreased, the range of unstable wave numbers is increased. In addition, for unstable wave numbers, the magnitude of the growth rate is increased.[14] These destabilizing effects can be seen in Eq. (6), where both $T$ and $G$ (which are stabilizing) are decreased with an increase in $\tau$ or $R$. Furthermore, an increase in viscosity is stabilizing since $G$ is the dominant term here (see Table 3). The dimensional wavelength data upon which Fig. 9 is based are shown in Fig. 10. These are the actual measured quantities taken from the motion picture film and are not based on boundary-layer calculations. The data show that in the low Reynolds number range, the wavelength increases until the more regular and slow waves are experienced.

It appears from the above observations that the supersonic pressure perturbation is the dominant instability mechanism in the low Reynolds number range and that the linear theory can predict data trends based on this mechanism.

### 3.3 Effect of Radius of Curvature and Mach Number

The effect of radius of curvature can be seen from comparing the wedge and cone data for similar conditions. From Figs. 6, 8, 11, and 12, the cone generally had a lower dimensionless and dimensional wave speed. More importantly, the observed wave number was smaller while $c_f(M^2 - 1)^{1/2} \approx 0.004$ for both the cone and wedge at the tunnel condition I given in Table 1. Interpreted in the light of the calculations in Sec. 3.2, the flow over the cone may be more unstable. A recent analysis,[29] based on the linear stability model described in Sec. 3.2 and including the ratio of the liquid depth to body radius, predicts this observation. All of the calculated cutoff wave numbers based on the experimental conditions are lower than those calculated using the two-dimensional model, which can be interpreted as destabilizing.

The effect of Mach number changes at constant shear (at test conditions I and III listed in Table 1) is inconclusive. The results of Nayfeh and Saric[14] showed that an increase in Mach number was stabilizing due to a reduction in the wave drag. However, because of blunt body effects, the boundary-layer edge Mach number was essentially identical for all of the runs. Examination of Figs. 6, 8, 11, and 12 shows that the $M = 7$ runs had lower dimensionless and higher dimensional wave speeds than the $M = 5$ runs, whereas the values of $\alpha$ and $\lambda$ were scattered within the experimental error.

## 4. Concluding Remarks

The experimental investigation of the response of a liquid film interacting with a laminar supersonic gas stream has been conducted using a blunt cone and a blunt wedge as models. Waves were observed under all circumstances. The wave speed and wave length were measured from high-speed motion pictures while the film properties were calculated using a newly developed liquid layer computer code.

The nondimensional wave speed was found to decrease monotonically with increasing $R$ from a value greater than the calculated interface velocity (fast waves) to a value lower than the calculated interface velocity (slow waves). The transition from fast waves to slow waves appeared to occur in the neighborhood of a Reynolds number of 100. The slow wave results were shown to be within an order of magnitude agreement with the Tollmien-Schlichting model of Miles.[15]

In the low Reynolds number range, the results were compared with an inviscid, supersonic external gas model[11,14] and agreement was found between the calculated and observed wave number and wave speed functional dependence on shear and Reynolds number. Furthermore, the Reynolds number and shear stress were found to be destabilizing, whereas the viscosity was found to be stabilizing.

The experimental data suggest that the liquid flow on a cone may be more unstable than that on the wedge. The effect of freestream Mach number was inconclusive because of blunt body effects.

## References

[1] Gater, R. L. and L'Ecuyer, M. R., "A Fundamental Investigation of the Phenomena that Characterize Liquid Film Cooling," Rept. TM-69-1, Jan. 1969, Jet Propulsion Center, Purdue Univ., Lafayette, Ind.

[2] Gold, H. and Pallone, A. J., "Interaction of a Surface Liquid Film and a Turbulent Gaseous Boundary Layer," *XXth Congress of the International Astronautical Federation*, Mar del Plata, Argentina, Oct. 1969.

[3] Gold, H., Mascola, R. E., and Smith, P. C., "Flow Characteristics of Porous Media and Surface Liquid Film Interactions," AIAA Paper 70-152, New York, 1970.

[4] Chandrasekhar, S., *Hydrodynamic and Hydromagnetic Stability*, Oxford University Press, 1961.

[5] Chang, I. D. and Russell, P. E., "Stability of a Liquid Layer Adjacent to a High-Speed Gas Stream," *The Physics of Fluids*, Vol. 8, 1965, pp. 1018–1026.

[6] Craik, A. D. D., "Wind-Generated Waves in Thin Liquid Films," *Journal of Fluid Mechanics*, Vol. 26, 1966, pp. 369–392.

[7] Benjamin, T. B., "Shearing Flow over a Wavy Boundary," *Journal of Fluid Mechanics*, Vol. 6, 1959, pp. 161–205.

[8] Miles, J. W., "On the Generation of Surface Waves by Shear Flow, Pt. 4," *Journal of Fluid Mechanics*, Vol. 13, 1962, pp. 433–438.

[9] Miles, J. W., "On the Generation of Surface Waves by Shear Flows," *Journal of Fluid Mechanics*, Vol. 3, 1957, pp. 185–204.

[10] Nayfeh, A. H. and Saric, W. S., "Non-Linear Kelvin-Helmholtz Instability," *Journal of Fluid Mechanics*, Vol. 46, 1971, pp. 209–232.

[11] Nachtsheim, P. R., "Analysis of the Stability of a Thin Liquid Film Adjacent to a High-Speed Gas Stream," TN D-4976, Jan. 1969, NASA.

[12] Nachtsheim, P. R., "Stability of Crosshatched Wave Patterns in Thin Liquid Films Adjacent to Supersonic Streams," *The Physics of Fluids*, Vol. 13, 1970, pp. 2432–2447.

[13] Nayfeh, A. H. and Saric, W. S., "Non-Linear Stability of a Liquid Film Interacting with a Supersonic Stream," Research Rept. SC-RR-710042, 1971, Sandia Corp., Albuquerque, N. Mex.

[14] Nayfeh, A. H. and Saric, W. S., "Stability of a Liquid Film," *AIAA Journal*, Vol. 9, No. 4, April 1971, pp. 750–752.

[15] Miles, J. W., "The Hydrodynamic Stability of a Thin Film of Liquid in Uniform Shearing Motion," *Journal of Fluid Mechanics*, Vol. 8, 1960, pp. 593–610.

[16] Hanratty, T. J. and Engen, J. M., "Interaction Between a Turbulent Air Stream over a Moving Water Surface," *American Institute of Chemical Engineers Journal*, Vol. 3, 1957, pp. 299–310.

[17] van Rossum, J. J., "Experimental Investigation of Horizontal Liquid Film," *Chemical Engineering Science*, Vol. 11, 1959, pp. 35–42.

[18] Cohen, L. S. and Hanratty, T. J., "Generation of Waves in the Concurrent Flow of Air and a Liquid," *American Institute of Chemical Engineers Journal*, Vol. 31, 1968, pp. 467, 479.

[19] Cohen, L. S. and Hanratty, T. J., "Effect of Waves at a Gas-Liquid Interface on a Turbulent Air Flow," *Journal of Fluid Mechanics*, Vol. 31, 1968, pp. 467–479.

[20] Plate, E. J., Chang, P. C., and Hidy, G. M., "Experiments on the Generation of Small Water Waves by Wind," *Journal of Fluid Mechanics*, Vol. 35, 1969, pp. 625–656.

[21] Kendall, R. M. and Bartlett, E. P., "Nonsimilar Solution of the Multicomponent Laminar Boundary Layer by an Integral-Matrix Method," *AIAA Journal*, Vol. 6, No. 6, June 1968, pp. 1089–1097.

[22] Grose, R. G. and Kendall, R. M., "The Homogeneous BLIMP with Liquid Layer Option—User's Guide," Rept. 70-3, Feb. 1970, Aerotherm Corp., Mountain View, Calif.

[23] Pate, S. R., "Measurements and Correlations of Transition Reynolds Numbers on Sharp Slender Cones at High Speeds," AEDC-TR-69-172, Dec. 1969, Arnold Engineering Development Center, Tullahoma, Tenn.

[24] Hendry, J. P., "Boundary-Layer Transition Correlation for Sharp Slender Cones," *Journal of Spacecraft and Rockets*, Vol. 3, No. 3, March 1966, pp. 426–427.

[25] Muir, J. F. and Trujillo, A. A., "Experimental Investigation of the Effects of Nose Bluntness, Free-Stream Unit Reynolds Number, and Angle of Attack on Boundary Layer Transition at a Mach Number of 6," Research Rept. SC-RR-710046, 1971, Sandia Corp., Albuquerque, N. Mex.

[26] Stetson, K. F. and Rushton, G. H., "Shock Tunnel Investigation of Boundary-Layer Transition at $M = 5.5$," *AIAA Journal*, Vol. 5, No. 5, May 1967, pp. 899–906.

[27] Softly, E. J., "Boundary Layer Transition on Hypersonic Blunt Slender Cones," AIAA Paper 69-705, San Francisco, 1969.

[28] Craik, A. D. D., *Wind-Generated Waves in Liquid Films*, Ph.D. dissertation, 1965, Univ. of Cambridge.

[29] Saric, W. S. and Gibbons, R. S., "Stability of Axisymmetric Liquid Films," Research Rept. SC-RR-710019, 1971, Sandia Corp., Albuquerque, N. Mex.

AUGUST 1971 AIAA JOURNAL VOL. 9, NO. 8

# An Analysis and Application of the Time-Dependent Turbulent Boundary-Layer Equations

HENRY MCDONALD* AND STEPHEN J. SHAMROTH†
*United Aircraft Research Laboratories, East Hartford, Conn.*

**The momentum and kinetic energy integral equations are derived for a compressible two-dimensional turbulent boundary layer with time-dependent mean velocity and density fields. The integral equations are used in conjunction with an assumed velocity profile family to predict the effect of small time-varying disturbances in the inviscid flow upon the behavior of a flat plate turbulent boundary layer. The prediction procedure is also used to investigate the possibility of dynamic coupling between small time-dependent disturbances in the inviscid flowfield and the resulting induced fluctuations arising from boundary-layer displacement effects. When applied to the flowfield resulting from a shock wave-boundary-layer interaction, the analysis predicts that certain disturbances couple with the boundary layer in an unstable manner and, thus, the analysis offers an explanation for an instability observed to occur in certain shock wave-boundary-layer interaction flowfields.**

## Nomenclature

$C_f$ = skin-friction coefficient
$H$ = shape factor
$L$ = dissipation length
$l$ = mixing length
$M$ = Mach number
$p$ = pressure
$q$ = turbulence intensity
$T_{\text{ad wall}}$ = adiabatic wall temperature
$T_{\text{wall}}$ = wall temperature
$t$ = time
$u$ = streamwise velocity
$u_c$ = convection velocity
$u_\tau$ = friction velocity
$u^*$ = Van Driest velocity
$v$ = transverse velocity
$x$ = streamwise coordinate
$y$ = transverse coordinate
$\delta$ = boundary-layer thickness
$\delta^*$ = displacement thickness
$\gamma$ = specific heat ratio
$\theta$ = momentum thickness
$\theta_E$ = kinetic energy thickness
$\theta_e$ = outer edge flow angle
$\theta_\rho$ = integral quantity defined by Eq. (12)
$\lambda$ = disturbance wavelength
$\rho$ = density
$\tau$ = shear stress
$\omega$ = disturbance frequency

***Subscripts***

$e$ = quantity evaluated at outer edge of boundary layer
$u$ = integral evaluated at constant density
$w$ = quantity evaluated at wall

Received May 7, 1970; revision received December 14, 1970. This investigation was sponsored in part by Pratt and Whitney Aircraft.

* Supervisor, Theoretical Gas Dynamics Group.

† Research Engineer, Theoretical Gas Dynamics Group. Associate Member AIAA.